IOP Publishing Journal of Physics: Conde
J. Phys.: Condens. Matter 37 (2025) 045502 (8pp) https://doi.org/10.1088/1

Hot carrier transfer from in Ag_{20} at H–Si(111) surface: TDDFT simulation in Wanni

John L Bost[1], Christopher Shepard[1] and Yosuke Kanai[1,2,*]

[1] Department of Chemistry, University of North Carolina at Chapel Hil of America
[2] Department of Physics and Astronomy, University of North Carolina a United States of America

E-mail: ykanai@unc.edu

Received 12 July 2024, revised 1 October 2024
Accepted for publication 25 October 2024
Published 11 November 2024

Abstract
Plasmon decay is believed to play an essential role in inducin interfaces between plasmonic nanoparticles and semiconducto employ real-time time-dependent density functional theory (Wannier gauge to gain quantum-mechanical insights into the no decay in the Ag_{20} nanoparticle at a semiconductor surface. The first-pr that the plasmon decay is more ... Ag_{20} ... a hydrogen-terminated Si(111) surface, taking place within 1 excitation. Hot carrier transfer across the interface is obse and nearly 30% of holes are generated deep in the valence band o The use of Wannier gauge in RT-TDDFT simulation is particularl quantum-mechanical insights into non-equilibrium electron heterogeneous systems.

Supplementary material for this article is available online

Keywords: plasmon, hot carriers, RT-TDDFT, interface, Wannier

1. Introduction

Plasmons, often viewed classically as collective oscilla tions of electron density, have been the subject of inten ive research. Quantum mechanically, plasmons are quasi particles that represent collective excitations of electrons they have been studied broadly in chemistry and condensed matter physics [1–8]. Plasmonic excitations are already central to various optical and photonic devices [9, 10], and various spectroscopic techniques, such as surface-enhanced Raman spectroscopy [11–13], ... take advanta nomenon. In more recent years, t ... has emerged as ... metal nanoparticles (NPs) has shown ... [14] ... [15, 16] ... efficiency for ... [2, 7, 17] ... [18, 19] ... [20–22] ... plasmonic NPs, there has been inc hot carrier generation [22–25] ... hot carriers are essential to pl [26, 27].

When plasmonic metal NPs are in ... semiconductor materials, the plasmon de

* Author to whom any correspondence should be addressed.

of excited charge carriers from the NP to the semiconductor [8, 28]. Developing a better understanding of the transfer mechanism is central to designing NP-semiconductor interfaces that enable plasmon-enhanced hot carrier transfer [29, 30]. However, despite the increasing interest in plasmon-induced charge transfer, its mechanism remains unclear [31, 32]. Naively, one might expect the fast decay of plasmon (e.g. Landau damping) and carrier relaxation (via phonons), followed by subsequent transfer of charge carriers (i.e. excited electrons and/or holes) across the interface. However, the experimentally observed ultrafast transfer time scale indicates the mechanism may not be due to such sequential steps. Hot (i.e. non-thermal) electron transfer has been reported to take place on a time scale faster than 100 fs, following the plasmon decay at such an interface [33, 34]. Theoretical calculations and spectroscopic measurements have suggested several quantum-mechanical mechanisms to explain such an ultra-fast process. Using first-principles calculation on the Au–TiO_2 interface, Prezhdo and co-workers proposed that efficient charge carrier transfer takes place across such a heterogeneous interface as a part of the plasmon decay process, since the plasmon already has a significant contribution from the semiconductor [35]. Lian and co-workers proposed, based on their spectroscopic studies on the interface of an Au NP and a CdSe nano-rod, a so-called plasmon-induced metal-to-semiconductor interfacial charge transfer transition (PICTT) mechanism. In this PICTT mechanism, the plasmon can decay by creating an interfacial electron-hole pair due to the strong mixing of the electronic states across the interface. Direct charge-transfer excitation across the interface could not explain their transient absorption measurements.

Given the complexity of the quantum mechanical processes involved, first-principles quantum dynamics simulations of electrons are poised to significantly advance our understanding of plasmon decay and possible charge carrier transfer processes arising from the nonlinear response at such interfaces [36, 37]. Using a prototypical NP-semiconductor interface between a silver NP and hydrogenated silicon semiconductor surface, we study the extent to which plasmon decay and carrier transfer can be coupled by employing real-time time-dependent density functional theory (RT-TDDFT). We employ the widely-used Ag_{20} cluster as a plasmonic NP [38, 39] and hydrogen-terminated Si(111) as the semiconductor surface. H–Si(111) is one of the most well-characterized and commonly synthesized semiconductor surfaces, offering the potential for future experimental comparison. Additionally, using H–Si(111) prevents unwanted effects, such as covalent bond formation, from being a factor in this study and deciphering interface effects. In this work, we take advantage of the recent development of RT-TDDFT method in the Wannier gauge [40, 41] so that only selected parts of the system can be intentionally excited; the maximally localized Wannier functions (MLWFs) on the NP are subjected to an external electric field to form a plasmonic excitation exclusively on the NP. In this way, we can ... excitation in a heterojunction interface ... isolated NP

2. Computational method

For simulations involving the Ag_{20} cluster and the ... interface, a ...
simulation ... was used ... 26 ... with the ...
the silver atoms taken from the ...
cluster ... Si(111) interface, ...
Si(111) surface was used with a ...
(see supporting information figure ...
tion energy of 0.13 eV for the Ag ...
consistent with having the inten...
istic details are unlikely to af...
transfer. A kinetic energy cutoff ...
for the plane-wave basis set to ...
orbitals along with periodic bo...
ulations. Hamann–Schluter–Chia...
norm-conserving [42] pseudopotentials ...
ver (17 valence electrons), sili...
hydrogen atoms. Given the intric...
we ensure the accuracy of the sim...
different levels of XC approxima...
calculations were performed wit...
PBE generalized gradient [43] ... approx...
additional calculations were re...
strained and appropriately norme...
is formulated to satisfy all know...
meta-GGA level [44]. A 0.025 atomic uni...
step with the enforced time-reversal [45] ...
was found to sufficiently converg...

All calculations were performed ...
ted within the Qb@ll code [46–51] ... simulation...
work were performed using RT-TDD...
[52]. In the Wannier gauge, the time-...
(KS) orbitals are represented as ...
more common Bloch function repre...
propagated throughout the RT-TDD...

$$i\frac{d}{dt}|w_i(t)\rangle = \left\{\hat{U}^{ML} + \frac{1}{2m}\left[-i\hbar\nabla\right]^2 + \hat{v}_{ext}(t) + \hat{v}_{HXC}[\{w_i(t)\}]\right\}|w_i(t)\rangle \quad (1)$$

where $\hat{U}^{ML}$ is the operator that ensures ...
the time-dependent MLWFs [41] ... external ...
tial due to the atomic nuclei and ...
$\hat{v}_{HXC}$ represents the Hartree and ex...
potentials. We note that converg...
was found to be particularly impo...
ing the plasmon excitation in the Wannier and i...
When a lower plane-wave energy cu...
qualitatively ... different ...
as shown in the supporting inform...

modeling the plasmonic exci... the more sophisticated non-e... approximation for validatio... approximation.

A time-dependent electric f... ic-ally excite the system with th... ial at a specific frequency,

$$(t) = {}_0\cos(\omega_0 t)\, e^{-\gamma(t-t_0)^2} \quad (2$$

where ω_0 is the excitation frequency, γ ... of the Gaussian ... t_0 ... amplitude/strength. The electr... rect... parallel to the surface throu... iting the MLWF repr... [41]. ... considered in this work as we... smon decay process. Subsequent ca... tron phonon scattering, takes pla... cale which is outside the scope of ... [53, 54].

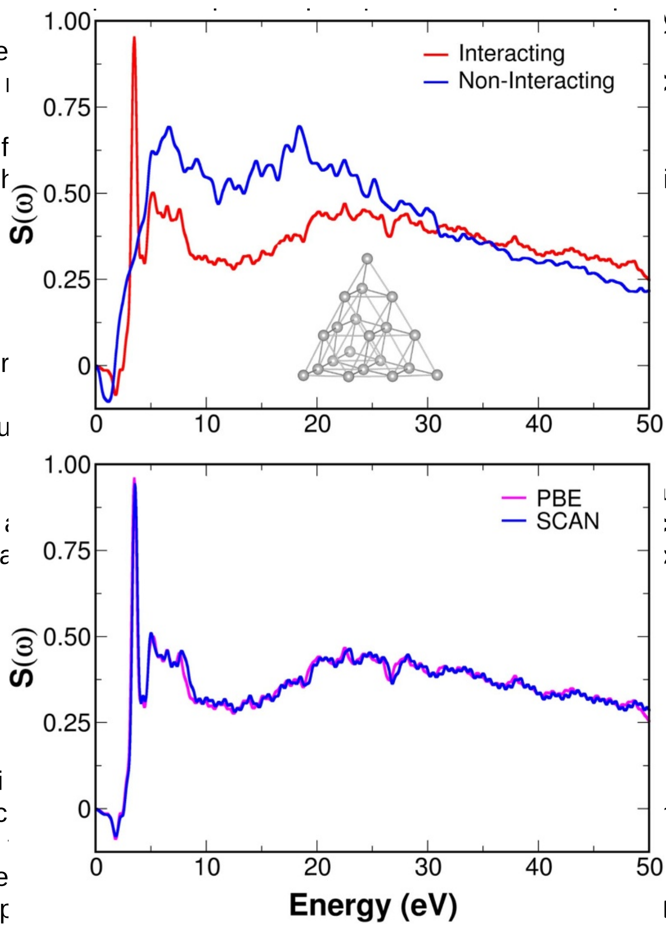

3. Results and discussion

3.1. Plasmon excitation

Following the work by ... [55], we identi... excitation peaks in the optic... isolated Ag_{20} cluster by eliminating ... r-actions such that both Hartre... ved and only the kinetic energy op... tion with ions are present in KS Hamiltonian. The optical absorption spectrum (in blue) for th... is shown in figure 1, together with the true optical absorption spectrum (in red). The prominent peak located at 3.5 eV in the absorption spectrum is absent when no electron–electron interactions are present and thus ... plasmon excitation [55]. This plasmon peak exists at 3.5 eV regardless of whether the PBE GGA or SCAN meta-GGA XC approximations are used, and it has been well documented in the literature [56–58]. Interestingly, the Wannier centers (expectation value of the position operator) located between the silver atoms are solely responsible for this peak, as shown in the supporting information (figure S3). In this work, we consider optical excitations at 3.5 eV and at 7.0 eV, of which the latter represents the usual non-plasmon excitation.

The external electric field at those specific frequencies of 3.5 eV and 7.0 eV was applied for 10 fs and the simulation was performed up to 50 fs to study the resulting excitation response. The number (i.e. population) of holes generated is calculated by projecting the TD-MLWFs onto the occupied KS eigenstates of the equilibrium system as

$$Ho(\varepsilon, t) = \sum_{i}^{occ.} 2 - 2\sum_{j}^{N} |\langle\psi_i|w_j(t)\rangle|^2 \delta(\varepsilon - \varepsilon_i) \quad (3)$$

where j refers to the index of the TD-MLWFs and ϕ_i ... KS eigenstates ε_i ... The total number of ... the number of excited electrons i...

Figure 1. (top) Comparison of the dipole ... absorption spectra of an isolated Ag_{20} ... RT-TDDFT simulations with (labeled ... (labeled 'non-interacting') electr... PBE GGA XC approximation. See text fo... Comparison of ... the PBE ... and the SCAN meta-GGA XC approximati...

... is obtained by integrating ... (3) ... ε_i of the valence band states. An a... used for calculating the excited ... ing sure that enough KS eigensta... (CB) are included in the integra... (2) and (c), as many as 800 eigenstat... (corresponding to 14.41 eV above ... the 7.0 eV non-plasmon excitatio... excited electrons are above the v... 800 CB eigenstates is not enough f... the excited electron population ... the holes. Both PBE GGA and SCAN me... imations yield quantitatively th... plasmon excitation, the observe... ferent. Being plasmonic in natur... and electronic excitation i...

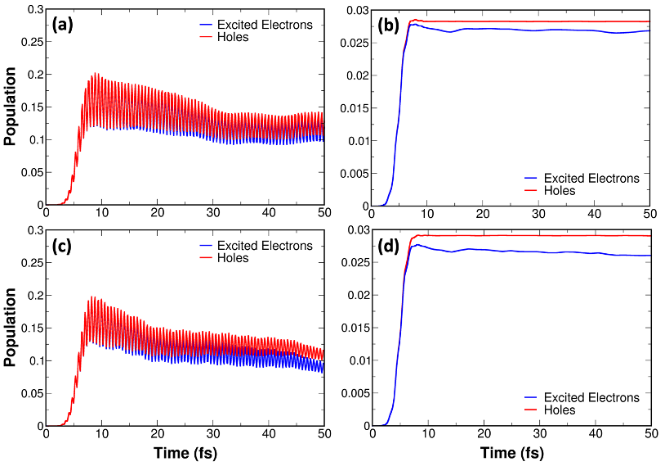

Figure 2. Holes and excited electrons … Ag_{20} nanoparticle with the electric field pulse at the excitation frequency of (a) 3.5 eV (plasmon) and (b) 7 eV (non-plasmon) using the PBE GGA XC approximation. The results using the SCAN XC approximation are also shown for the (c) 3.5 eV (plasmon) and (d) 7 eV (non-plasmon). Note the y-axis is 10× larger for the plasmon cases (a) and (c) because of the significantly larger cross section for the plasmon excitation. The calculated population of the excited electrons here can be less than that of the holes because a finite number of virtual orbitals (800 eigenstates, covering 14.41 eV above LUMO) were used to quantify the excited electrons.

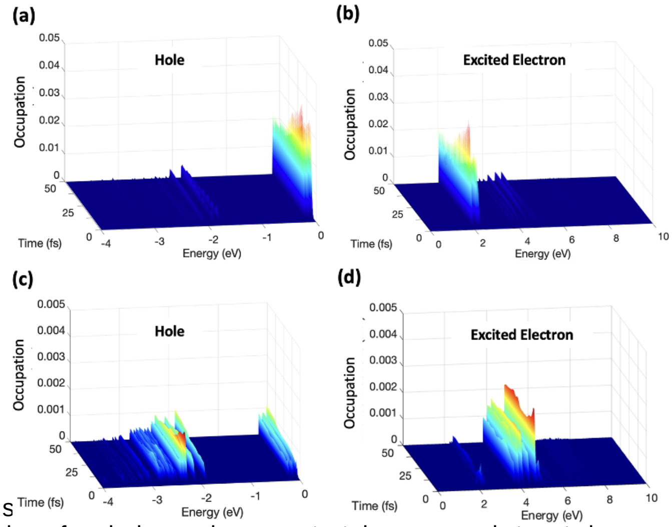

Figure 3. Occupation of the charge carriers … equilibrium KS eigenstates of Ag_{20} NP: (a) and (b) for the plasmonic excitation (3.5 eV) … (c) and (d) for the non-plasmonic excitation (7 eV). The … orbital (HOMO) is set to 0 eV.

of magnitude. Notably, the population of the excited carriers (holes and excited electrons) rapidly oscillates with a frequency of 0.60 fs even without atomic movements, which are purposely absent in this RT-TDDFT simulation. While this rapid oscillation does not necessarily define the plasmon quantum-mechanically, it is consistent with the classical view of oscillating charge density. Unlike the non-plasmon excitation, the numbers of carriers gradually decrease after the external electric field is turned off. Note that the number of holes and the excited electrons within the 800 CB eigenstates are initially the same. However, with time, these two quantities deviate from each other, indicating that some excited electrons become more energetic than 14.41 eV above LUMO (beyond 800 CB eigenstates, figure 2). Also, the oscillation magnitude tends to become smaller, indicative of plasmon decay, as the carrier population gradually trends toward a plateau. Using the SCAN meta-GGA XC approximation, the timescale of the oscillation decay and the oscillation frequency are qualitatively on the same scale as the simulation using the PBE GGA XC approximation.

Excited electron and hole generation can be examined in terms of the KS energy because the projected states ϕ_i in equation (3) are the KS eigenstates. Figure 3 shows the quantum dynamics of electrons in terms of how the occupation of the KS eigenstates changes in time and energy. For the non-plasmonic excitation, the electronic excitation produces excited electron amplitudes around 5 eV above HOMO and hole amplitudes around 2 eV below HOMO. There are no notable time-dependent changes as shown in figure 2. On the other hand, figure 3 shows only a few eigenstates close to the HOMO–LUMO energy gap are responsible for the plasmonic excitation. Once the field is turned off at 10 fs, the excited electrons and holes are generated at higher (∼4 eV) and deeper (∼−2 eV) energies, respectively. It is interesting to note that particularly the … remains constant after the … (supporting information, figure S…). Both the excited electrons and holes … relatively far from the band edge … speaking, the generation of hot … the decreasing number of … higher energies. Quantitatively … for the SCAN XC approximation (see figure S7).

To understand this observation … tion while no such behavior is observed … excitation, we need to consider … single-particle energies. In RT-… energy can be expressed as

$$E(t) = \sum_i^N \langle \phi_i(t) | \hat{H}_{KS}[\{\phi_i(t)\}] | \phi_i(t) \rangle + \sum_i^N \langle \phi_i(t) | \varepsilon_{xc} - v_{xc} | \phi_i(t) \rangle - E_{es}[\{\phi_i(t)\}] \quad (4)$$

where ε_{xc} is the XC energy density and … E_{es} is the electrostatic energy. By neglecting the dependence ($\hat{H}_{KS}[\{\phi_i(t)\}]$) on the TD-KS orbitals, the … be expressed as

$$E(t) \approx \sum_s \sum_i^N |\langle \psi_s | \phi_i(t) \rangle|^2 \varepsilon_s + \sum_i^N \langle \phi_i(t) | \varepsilon_{xc} - v_{xc} | \phi_i(t) \rangle - E_{es}[\{\phi_i(t)\}] \quad (5)$$

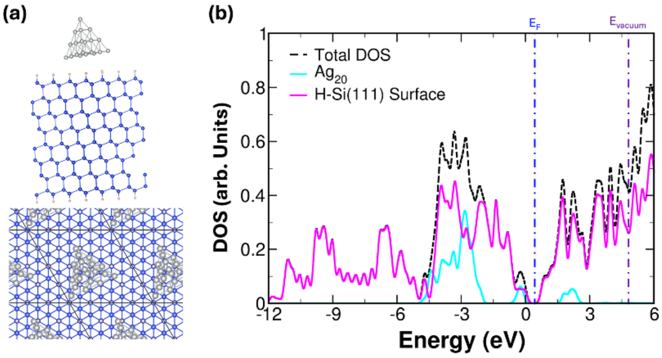

Figure 4. (a) Model of the Ag_{20} NP on the H–Si(111) surface from the side a… density of states (PDOS) of the i… molecular orbital (HOMO) was set … broadening of 0.15 eV was used. The Fermi and vacuum energy levels are denoted by blue and violet dashed lines, respectively.

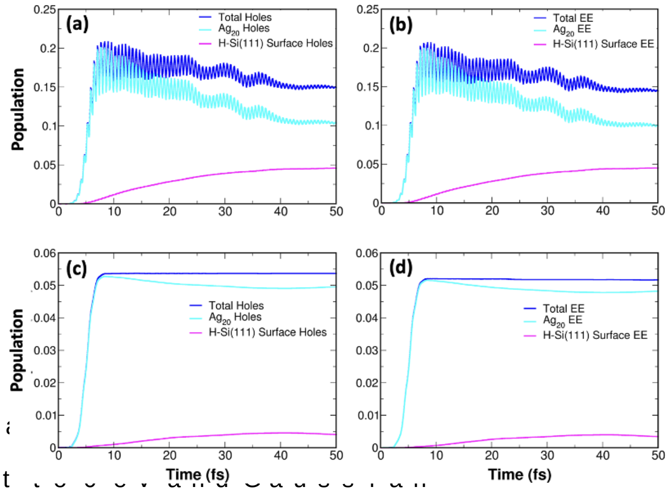

Figure 5. Population changes of the Ag_{20}/H–Si(111) interface for the (a) holes and (b) excited electro[ns at] the plasmonic excitation frequency … changes for the (c) holes and (d) exc[ited electrons at the] non-plasmonic excitation frequency. [The populations] are decomposed in terms of the Ag_{20} and the H–Si(111) surface.

Thus, the total energy can be … single-particle energy ϵ_j weighted by the occu[pation] … pation (the first term) and additional XC-contributing and elec-trostatic energy terms. The total energy remains constant aft[er] the external electric field is turned off at 10 fs. The XC and electrostatic contributions … on ex[cit]ation (figure 1); the plasmon peaks ar[e] … absorption spectrum without t[he] … the XC and electrostatic contribut[ions] … [p]lasm[on] decay which yields hot carrie[rs].

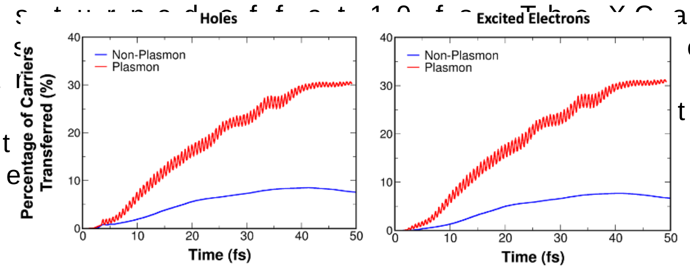

Figure 6. Percentage of generated charge [carriers] transferred from the Ag_{20} NP to the H–Si(111) inter[face for] plasmonic and non-plasmonic excitatio[n] … charge carriers generated is much la[rger] …

3.2. Ag_{20} NP on H–Si(111) surface

Let us now discuss how the plasmon decay could potentially affect the charge/energy transfer at the Ag_{20}–Si(111) interface. Given that the PBE GGA and SCAN meta-GGA calculations yield essentially the same results (see supporting information, figures S8–S11), we only discuss the results from using the PBE GGA XC approximation in this section. The projected density of states (PDOS) for the Ag_{20}–Si(111) interface (figure 4(b)) shows a type-I heterojunction … HOMO and the LUMO localized on the silicon surface … figure 4 … The large DOS from the silicon … [illegible] … figures 5 and 6. … ity for the excitation transfer … tially excited plasmon nanoparticle. … the first 10 fs of the RT-TDDFT simulation, the external electric field … excite only the Ag_{20} nanoparticle. This is possible because the type-I sta… single-particle states are r… (figure 4) … Ag_{20} NP … MLWFs. Since all the time-dependent MLWFs are spatially … localized either on the Ag_{20} nanoparticle or on H–Si(111) surface, the excited electron and hole populations … separately for individual … figure 5 … As … shown in figure 5 … expected, the plasmon excitation … is four times larger than that … Figure 6 shows the percentage of charge carriers … the semiconductor, and the plasmonic excitation … increased carrier generation … transferred charge carriers. … tion period is 0.60 fs in the case …

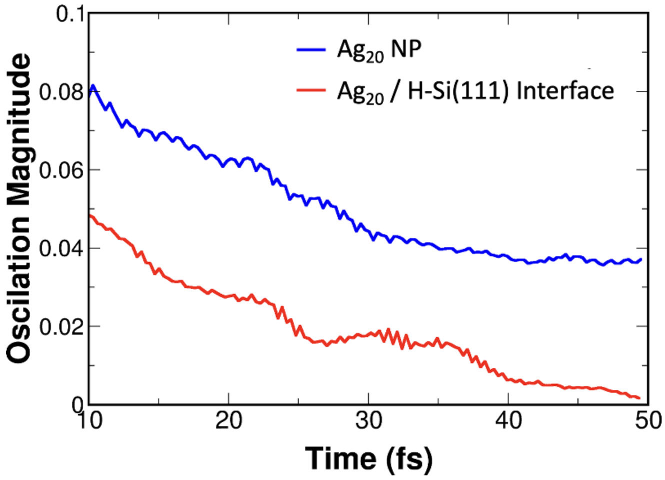

Figure 7. Magnitude of the plasmon-de[illegible] population of charge [illegible] (Ag$_{20}$ NP) and [illegible] figure 5 [illegible] (Ag$_{20}$/H–Si(111) interface). At 10 [illegible] is turned off and the plasmon begins [illegible]

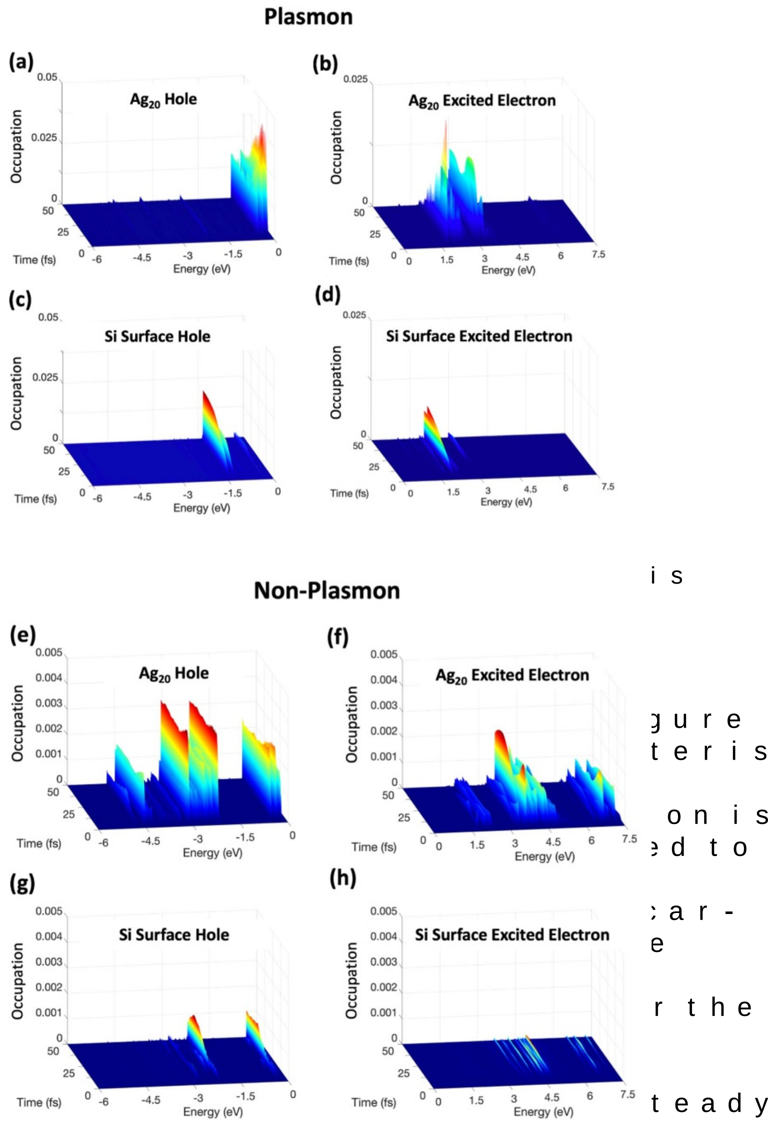

slightly longer (6.3 fs) for Ag$_{20}$ NP [illegible] period is identical for exci[illegible] 7 [illegible] gure quantifies the magnitude of th[illegible] ter is oscillation in Ag$_{20}$ NP persists for [illegible] than 50 fs while the plasmoni[illegible] on is largely diminished by 50 fs a[illegible] ed to the semiconductor.

To gain further insights, t[illegible] car- riers is given in terms of KS e[illegible] 8 [illegible] e. As in the case of Ag$_{20}$ NP, the excited [illegible] hole generations occurs over [illegible] r the non-plasmonic excitation (figure 8(e)–(h)) [illegible] excitation (figure 8(a)–(d)), even aft[illegible] tric field is switched off, th[illegible] teady increase in the energy range around 3 eV as a secondary effect.

As in the case of Ag$_{20}$ NP, [illegible] carrier generation [illegible] Ag$_{20}$ NP [illegible] within 3 eV [illegible] At the same time, the magnitude [illegible] eration is much larger than [illegible] NP (see figure 3). This is consistent w[illegible] the plasmon decay occurs on a mu[illegible] interface than in the isolated [illegible] semiconductor side, the occupations start to increase as a res ult of the carrier transfer [illegible] excites electrons [illegible] shows the most prominent increase [illegible] 1.5 eV, close to the energies of [illegible] in the Ag$_{20}$ NP for the plasmon excitation [illegible] small in magnitude, there is a [illegible] occupations around 3 eV for the [illegible] that many of the excited e[illegible] by the plasmon excitation are [illegible] the observation of hot carri[illegible] its small magnitude. For the h[illegible] rier transfer at this interface [illegible] <10 fs. [illegible] occupations increase ra[illegible]

[illegible] occupation of the charge carrie[illegible] equilibrium KS eigen[illegible] Ag$_{20}$/H–Si(111) [illegible] decomposed into contributions from Ag$_{20}$ NP and (c)–(d) the H–Si(111) surface for th[illegible] and (e)–(f) [illegible] surface [illegible] non-plasmonic excit[illegible] [illegible] highest occupied [illegible] (HOMO) [illegible]

4. Conclusion

In this work, we employed the recently developed RT-TDDFT method in the Wannier gauge to investigate plasmon decay and the possibility of hot carrier transfer at the interface between an Ag_{20} nanoparticle and H–Si(111) surface. We simulate the electronic excitation process from an external electric field and study the nonlinear response of electrons over time at two different frequencies, one corresponding to the plasmonic excitation and the other corresponding to an ordinary optical excitation. Our first-principles simulations show that the plasmon decay is accelerated at the interface, taking place within 100 fs of the plasmon excitation. Concurrently, hot carrier transfer across the interface was observed as a result of the plasmon decay process, and a significant number of holes are generated deep in the valence band of the semiconductor surface. RT-TDDFT simulation in the Wannier gauge is a promising first-principles approach for gaining quantum-mechanical insights of various non-equilibrium electron dynamics in complex heterogeneous systems.

While this work provides further insights into the quantum-mechanical details of hot carrier transfer from plasmon decay, additional investigation into subsequent carrier relaxation is required to fully understand the non-linear dynamics on the picosecond timescale. Additionally, exploring other plasmonic NPs could offer further insights into the initial decay process [59]. Finally, modern spectroscopic techniques, such as ultrafast transient absorption, are expected to provide experimental validation for the plasmon decay timescales [34, 60].

Data availability statement

All data that support the findings of this study are included within the article (and any supplementary files).

Acknowledgments

This work was supported by the National Science Foundation under No. CHE-1954894.

ORCID iDs

John L Bost https://orcid.org/0009-0002-9783-7028
Christopher Shepard https://orcid.org/0000-0002-3604-414X
Yosuke Kanai https://orcid.org/0000-0002-2320-4394

References

[1] Jablan M, Buljan H and Soljačić M 2009 Plasmonics in graphene at infrared frequencies Phys. Rev. B 80 245435
[2] Atwater H A and Polman A 2010 Plasmonics for improved photovoltaic devices Nat. Mater. 9 205–13
[3] Ritchie R H 1973 Surface plasmons in solids Surf. Sci. 34 1–19
[4] Economou E N 1969 Surface plasmons Phys. Rev. 539–54
[5] Garcia M A 2011 Surface plasmons in fundamentals and applications J. Phys. D: Appl. Phys. 283001
[6] Halas N J, Lal S, Chang W-S, Link S a Plasmons in strongly coupled met Chem. Rev. 3913–61
[7] Thomann I, Pinaud B A, Chen Z, Clem and Brongersma M L 2011 Plasmon en energy conversion Nano Lett. 3440–6
[8] Hattori Y, Meng J, Zheng K, Meier d Broqvist P, Nordlander P and Sá carrier generation in plasmonic Nano Lett. 1083–9
[9] Nie S and Emory S R 1997 Probing sin single nanoparticles by surface Science 1102–6
[10] Peyser L A, Vinson A E, Bartko A P an Photoactivated fluorescence fro nanoclusters Science 103–6
[11] Somekh M G, Liu S, Velinov T S and Se High-resolution scanning surfac Appl. Opt. 6279–87
[12] Willets K A and Van Duyne R P 2007 Lo plasmon resonance spectroscopy Annu. Rev. Phys. Chem. 267–97
[13] Gao W, Huang T, Xu X H and El-sayed-A Localized surface plasmon reson nanoparticles studied by dark-f spectros. J. Appl. Phys. 34310
[14] Schaadt D M, Feng B and Yu E T 2005 En semiconductor optical absorptio excitation in metal nanoparticl Appl. Phys. Lett. 063106
[15] Jain P K, Huang X, El-Sayed I H and E Review of some interesting surfa resonance-enhanced properties and their applications Plasmonics 107–18
[16] Wang L, Hasanzadeh Kafshgari M and Optical properties and applicat nanoparticles Adv. Funct. Mater. 2005400
[17] Linic S, Christopher P and Ingram D nanostructures for efficient con energy Nat. Mater. 911–21
[18] Christopher P, Xin H and Linic S 20 catalytic oxidation reactions o nanostructures Nat. Chem. 467–72
[19] Marimuthu A, Zhang J and Linic S 20 propylene epoxidation by plasmo photo-switching Cu oxidation Science 1590–3
[20] Knight M W, Sobhani H, Nordlander P Photodetection with active opti Science 702–4
[21] Brongersma M L, Halas N J and Nordl Plasmon-induced hot carrier sci Nat. Nanotechnol. 25–34
[22] Manjavacas A, Liu J G, Kulkarni V an Plasmon-induced hot carriers in ACS Nano 7630–8
[23] Román Castellanos L, Hess O and Lis plasmon hot carrier generation i Commun. Phys. 47
[24] Mohammadi M, Vempurpoal A, Tordera D, Schmidt-Ott A and Smith W A 2017 H and extraction of plasmonic allo ACS Photon. 1146–52

[25] Lee H, Park Y, Song K and Park J Y 2022 … plasmon-induced hot carriers: … applications Acc. Chem. Res. … 3727–37
[26] Christopher P and Moskovits M 2017 … transmission from pl[illegible] Annu. Rev. Phys. Chem. … 379–98
[27] Song K, Lee H, Lee M and Park J Y 2021 … hole-driven water splitting on Au nanoparticles/p-type GaN … ACS Energy Lett. … 1333–9
[28] Narang P, Sundararaman R and Atwater H A 2016 … hot carrier dynamics in solid-state … energy conversion Nanophotonics … 96–111
[29] Sundararaman R, Narang P, Jermyn A S, Goddard W A and Atwater H A 2014 Theoretical predictions for hot-carrier generation from surface plasmon decay Nat. Commun. … 5788
[30] Clavero C 2014 Plasmon-induced hot-electron generation at nanoparticle/metal-oxide interfaces for photovoltaic and photocatalytic devices Nat. Photon. … 95–103
[31] Hartland G V, Besteiro L V, Johns P and Govorov A O 2017 What's so hot about electrons in metal nanoparticles? ACS Energy Lett. … 1641–53
[32] Moon C W, Choi M-J, Hyun J K and Jang H W 2021 Enhancing photoelectrochemical water splitting with plasmonic Au nanoparticles Nanoscale Adv. … 5981–6006
[33] Du L, Furube A, Yamamoto K, Hara K, Katoh R and Tachiya M 2009 Plasmon-induced charge separation and recombination dynamics in gold–TiO_2 nanoparticle systems: dependence on TiO_2 particle size J. Phys. Chem. C … 6454–62
[34] Wu K, Chen J, McBride J R and Lian T 2015 Efficient hot-electron transfer by a plasmon-induced interfacial charge-transfer transition Science … 632–5
[35] Long R and Prezhdo O V 2014 Instantaneous generation of charge-separated state on TiO_2 surface sensitized with plasmonic nanoparticles J. Am. Chem. Soc. … 4343–54
[36] Kumar P V, Rossi T P, Marti-Dafcik D, Reichmuth D, Kuisma M, Erhart P, Puska M J and Norris D J 2019 Plasmon-induced direct hot-carrier transfer at metal–acceptor interfaces ACS Nano … 3188–95
[37] Rossi T P, Erhart P and Kuisma M 2020 Hot-carrier generation in plasmonic nanoparticles: the importance of atomic structure ACS Nano … 9963–71
[38] Asadi-Aghbolaghi N, Rüger R, Jamshidi Z and Visscher L 2020 TD-DFT+TB: an efficient and fast approach for quantum plasmonic excitations J. Phys. Chem. C … 7946–55
[39] Giannone G and Della Sala F 2020 Minimal auxiliary basis set for time-dependent density functional theory and comparison with tight-binding approximations: application to silver nanoparticles J. Chem. Phys. … [illegible]
[40] Gygi F, Fattebert J-L and Schwegler E 2003 Computation of maximally localized Wannier functions using a simultaneous diagonalization algorithm Comput. Phys. Commun. … 1–6
[41] Yost D C, Yao Y and Kanai Y 2019 Propagation of maximally localized Wannier functions in real-time TDDFT J. Chem. Phys. … 194113
[42] … Schlüter M and Chiang C … Phys. Rev. Lett. … 1494–7
[43] … Burke K and Ernzerhof M … gradient approximation … Phys. Rev. Lett. … 3865–8
[44] … Ruzsinszky A and Perdew J P 2 … Phys. Rev. Lett. … 036402
[45] … H A 2016 Plasmon … and Rubio A 2 … Chem. Phys. … 3425–33
[46] … Gygi F … Qbox code … Lawrence Livermore National L…
[47] Schleife A, Draeger E W, Kanai Y and … Plane-wave pseudopotential imp… time-dependent … Chem. Phys. … 22A546
[48] Schleife A, Draeger E W, Anisimov V … and Correa A A 2014 Quantum dynamics sim… Comput. Sci. Eng. … 54–60
[49] … 2022 Electron dynamics in … real-time time-dependent … MRS Commun. … 1002–14
[50] Shepard C, Zhou R, Yost D C, Yao Y and Kanai Y 2021 Simulating electronic excitation … approach … plane-wave pseudopotential … J. Chem. Phys. … 100901
[51] Xu J, Carney T E, Zhou R, Shepard C and Kanai Y 2024 Real-time time-dependent density … J. Am. Chem. Soc. … 5011–29
[52] Marzari N and Vanderbilt D 1997 Maximally localized generalized Wannier functions f… Phys. Rev. B … 12847–65
[53] Zhang Y 2021 Theory of plasmonic ho… J. Phys. Chem. C … 9201–8
[54] Zhou J G, Zhang … 2019 …, Link S and Nordlan… ACS Photonics … 2584–95
[55] Ma J, Wang Z and Wang L-W 2015 Inter… Nat. Commun. … 10107
[56] Lethiec C M, Madison L R and Schatz … on the acoust… (20, 84 and 120) … J. Phys. Chem. … 20572–8
[57] Aikens C M, Li S and Schatz G C 2008 … (35, 56, 84, 120) … J. Phys. Chem. C … 11272–9
[58] Ma J and Gao S 2019 Plasmon-induced … TiO_2(110) … ACS Nano … 13658–67
[59] … Kim J-M, Park J-E and Nam J-M … Nonnoble-metal-based plasmonic … Adv. Mater. … 1704528
[60] … 2024 TDDFT … role of the plasmon … charge … Sci. Adv. … eadp3353